Radio Frequency Scanning Tunneling Spectroscopy for Single-Molecule Spin Resonance

Stefan Müllegger,[1,*] Stefano Tebi,[1] Amal K. Das,[1,†] Wolfgang Schöfberger,[2] Felix Faschinger,[2] and Reinhold Koch[1]
[1]*Institute of Semiconductor and Solid State Physics, Johannes Kepler University Linz, 4040 Linz, Austria*
[2]*Institute of Organic Chemistry, Johannes Kepler University Linz, 4040 Linz, Austria*
(Received 3 July 2014; published 25 September 2014)

We probe nuclear and electron spins in a single molecule even beyond the electromagnetic dipole selection rules, at readily accessible magnetic fields (few mT) and temperatures (5 K) by resonant radio-frequency current from a scanning tunneling microscope. We achieve subnanometer spatial resolution combined with single-spin sensitivity, representing a 10 orders of magnitude improvement compared to existing magnetic resonance techniques. We demonstrate the successful resonant spectroscopy of the complete manifold of nuclear and electronic magnetic transitions of up to $\Delta I_z = \pm 3$ and $\Delta J_z = \pm 12$ of single quantum spins in a single molecule. Our method of resonant radio-frequency scanning tunneling spectroscopy offers, atom-by-atom, unprecedented analytical power and spin control with an impact on diverse fields of nanoscience and nanotechnology.

DOI: 10.1103/PhysRevLett.113.133001 PACS numbers: 33.20.-t, 33.25.+k, 33.35.+r, 68.37.Ef

Experimental detection of nuclear and electron spin excitation by a resonant magnetic field oscillating in time [1,2] is restricted by (i) a sensitivity limit of about 10^{10} spins, thus complicating spin control in individual atoms and molecules essential for quantum computation and spintronics [3], (ii) the fundamental electromagnetic dipole selection rules impeding the detection of high-spin transitions in single-molecule magnets and metallorganic molecular agents [4], and (iii) the lack of subnanometer spatial resolution, hiding intramolecular details of single functional (bio)molecules [5–7]. Our new approach, based on electron-induced spin excitation, overcomes all these limitations simultaneously.

Classical electron- and nuclear-magnetic resonance methods utilize electromagnetic fields to excite electron and nuclear spin transitions. Furthermore, an electric current in a magnetic system can efficiently excite its magnetic moments, as well. For instance, dc electron tunneling has been demonstrated to excite magnons [8], flip the spin of a single atom [9,10], or switch on and off molecular spins [11] by inelastic processes. Radio-frequency (rf) currents through nanoscale magnetic bars have been shown to excite ferromagnetic resonance [12]. Current-noise measurements by a scanning tunneling microscope (STM) have enabled the detection of single electron spins in surface dangling bonds [13–15], adatom clusters [16], and molecular clusters [17]; the transient and extremely small spin-noise signals necessitate sophisticated rf circuitry and often extensive data accumulation [14]. However, a spectroscopic spin resonance method based on rf current with true single-molecule sensitivity (i.e., probing one molecule at a time) and subnanometer spatial resolution, has so far not been achieved.

Herein, we demonstrate the resonant probing of electronic and nuclear spin transitions in a single magnetic molecule with subnanometer spatial resolution, and beyond the electromagnetic dipole selection rules, e.g., with $\Delta J_z = \pm 12$ and $\Delta I_z = 0, \pm 1, \pm 2, \pm 3$ for the change of electronic and nuclear spin projections, respectively. The present work is based on simultaneous dc tunneling through electronic levels of a single magnetic molecule while superposing an additional rf tunneling current for resonant spin excitation in a weak static magnetic field [Fig. 1(a)]. For this purpose, we adapted a conventional STM (Createc) with a dedicated homebuilt rf excitation circuit. Tuning the rf component in resonance with a molecular spin-flip transition, i.e., $h\nu_{\mathrm{rf}} = |E(\uparrow) - E(\downarrow)|$, is found to significantly modify the dc tunneling conductance. This effect, so far unobserved, enables a new type of "magnetic resonance" spectroscopy based on conductance measurement during rf excitation at μeV energies and readily accessible magnetic fields (few mT) and temperatures (5 K). We denote this novel technique herein as rf scanning tunneling spectroscopy (rf-STS).

The feasibility of our rf-STS method for resonant spin spectroscopy is demonstrated for single molecules of the "terbium double decker" bis(phthalocyaninato)terbium(III) ($TbPc_2$, Fig. 1). $TbPc_2$ consists of a Tb^{3+} ion sandwiched between two organic phthalocyanine ligands [18,19]. According to Hund's rules, the Tb^{3+} ion has an electronic spin of $S = 3$ and orbital angular momentum of $L = 3$; strong spin-orbit coupling yields a total electronic angular momentum of $J = 6$. Because of the unusually high ligand field induced by the two phthalocyanine ligands (negative axial zero-field splitting) the electron-spin ground state doublet of $J_z = m_J = \pm 6$ is separated by more than 50 meV from the next higher doublet of $J_z = \pm 5$ [18–21]. This property makes $TbPc_2$ an exceptional single-molecule magnet [4] that behaves like an Ising spin at temperatures up to ≈ 100 K [19]. At avoided level

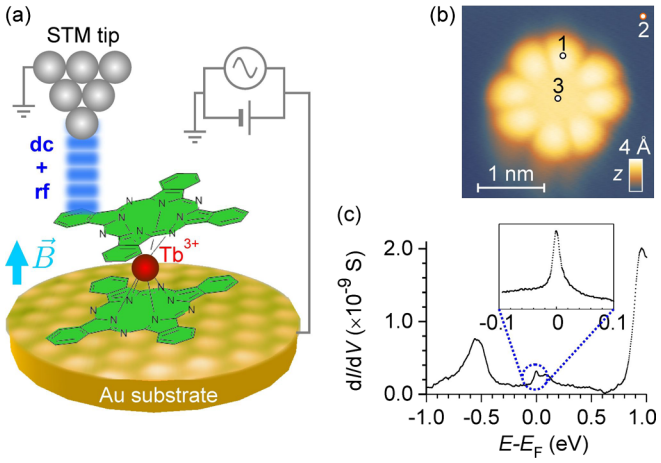

FIG. 1 (color online). (a) Schematic experimental setup of radio frequency scanning tunneling spectroscopy (rf-STS) on a single molecule; a terbium-double decker molecule $[TbPc_2]^0$ resides inside the STM tunnel junction formed by the tip and Au(111) substrate; the Tb^{3+} ion (red) is sandwiched between two phthalocyanine ligands (green); a static magnetic field is applied perpendicular to the substrate surface; dc and rf components of the tunneling current are simultaneously applied by separate sources. (b) STM topographic image of a $TbPc_2$ molecule adsorbed on Au(111) at 5 K (+1 V, 100 pA); circles mark different tip positions over the ligand (1) and center (3) of the molecule as well as over the bare substrate surface (2). (c) dI/dV spectrum of $TbPc_2$/Au(111) at dc tunnel conditions measured at position 1; inset: characteristic Kondo signature of the neutral $[TbPc_2]^0$ molecule on Au(111) observed by dc tunneling spectroscopy.

crossings, quantum tunneling of magnetization enables magnetization reversal [20].

In addition to the electronic angular momentum J, the Tb^{3+} ion carries a nuclear spin of $I = 3/2$. According to a model spin Hamiltonian proposed by Ishikawa *et al.* [19,20], which is considered as well established in the literature [22–25], I and J are coupled by a large hyperfine interaction (dipole and quadrupole). The resulting fourfold nonequidistant splitting of each electronic spin level of Tb^{3+} is illustrated in Fig. 2(a) by the Zeeman diagram of the lowest $J_z = \pm 6$ substates of the $J = \pm 6$ ground-state doublet. The hyperfine levels, labeled $|J_z, I_z\rangle$, are obtained by numerical diagonalization of Ishikawa's spin Hamiltonian with the software EASYSPIN [26]. Notice, that Fig. 2(a) refers to negatively charged $[TbPc_2]^-$, which we regard as a suitable model system for the presented rf-STS experiments. Our measurements show that rf-STS necessitates tunneling into unoccupied electronic states of neutral $[TbPc_2]^0$ (see below), thereby temporarily charging the molecule negatively. From the Zeeman diagram of Fig. 2(a) one expects nine spin transitions of $TbPc_2$ to lie within our experimental bandwidth of 4.2 GHz. The calculated frequency values are plotted on the abscissae of Fig. 2(b) for magnetic field values of 2.5 and 16 mT, respectively. Three hyperfine transitions, labeled 1–3, are purely nuclear with $\Delta I_z = \pm 1$ and the electron angular momentum being conserved ($\Delta J_z = 0$)—see yellow, green and blue arrows in Fig. 2(a). These transitions depend only weakly on the magnetic field (nuclear Zeeman effect) due to the large proton-to-electron mass ratio of ≈1836. On the contrary, purely electronic transitions and mixed electronic-nuclear transitions are considerably Zeeman shifted. This is clearly seen by comparing the respective transition frequencies labeled 4 (4′) and 5 (5′). Figure 2(b) summarizes our main experimental result: the detection of rf-STS signals—plotted on the ordinate—on single $TbPc_2$ molecules that agree within ±8% with the calculated spin transitions plotted on the abscissa.

In the following, we discuss in detail the experimental conditions of our rf-STS measurements on $TbPc_2$. $TbPc_2$ molecules were synthesized by the procedure reported in Refs. [27,28] followed by purification in a column chromatograph with silica gel and toluene as an eluent. The single-crystal Au(111) substrate was prepared by repeated cycles of Ar^+ ion bombardment and annealing at 700 K. $TbPc_2$ was thermally evaporated at ultrahigh vacuum conditions from a quartz crucible at 700 K after thorough degassing for > 12 h at 363 K and < 1 h at 473 K. The rf-STM has been employed recently by our group for the successful detection of rf tunneling current signals in the 100-MHz regime for detecting and exciting the mechanical motion of molecules [29,30]. STM and rf-STS experiments were performed with electrochemically etched W tips deoxidized by annealing in vacuum. Impurity and tip effects were minimized by multiple tip forming between the experiments, resulting in Au-coated tips. Reliable tip performance was established by accurately reproducing the characteristic conductance signature of the Au(111) surface state well known in the literature [31].

We have studied single neutral $[TbPc_2]^0$ molecules adsorbed on Au(111) at 5 K with the phthalocyanine planes aligned parallel to the substrate surface [32]. Figure 1(b) shows the characteristic STM topographic appearance with a symmetric 8-lobe structure [11,33]. $[TbPc_2]^0$ molecules on Au(111) are clearly identified by a characteristic Kondo signature [34] observed by dc tunneling spectroscopy [see Fig. 1(c)]. It originates from an open-shell π system on the phthalocyanine ligands with an electronic spin of $S = 1/2$, while being absent in $[TbPc_2]^-$ anions [11]. The dI/dV signal was obtained by lock-in technique with sinusoidal modulation of the sample voltage at 704 Hz and 10–20 mV peak to peak.

For the rf-STS resonance experiments, a sinusoidal ac tunneling voltage from a rf signal generator is coupled in via a bias tee to the sample (for further details see Ref. [30]). In the present work, we utilize high-grade rf elements for achieving an experimental bandwidth of 4.2 GHz. The resulting rf current does not significantly affect the tunnel distance, because the radio frequency is

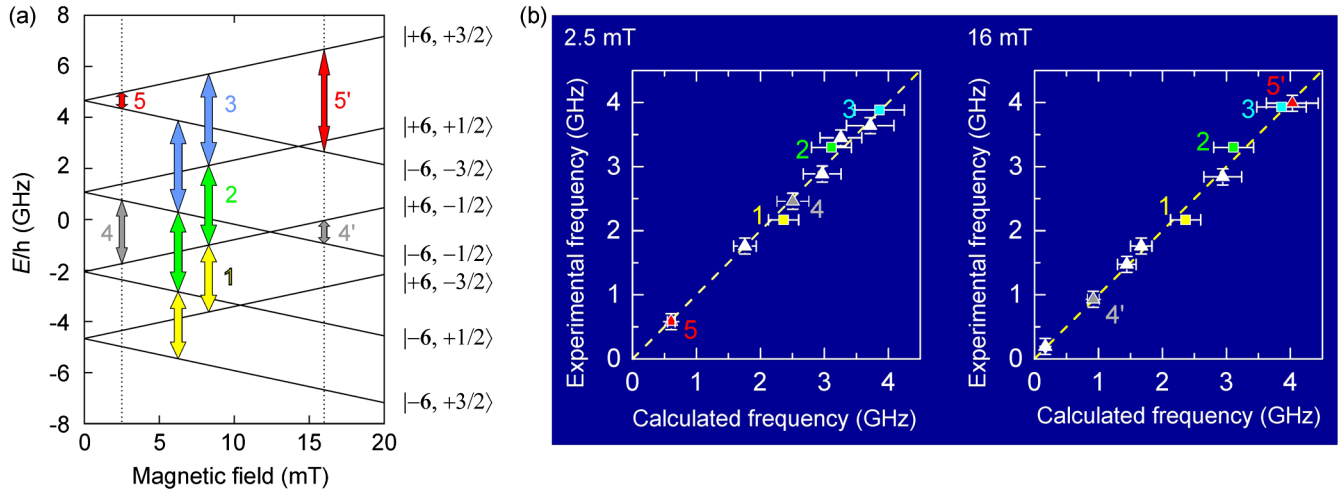

FIG. 2 (color online). Nuclear and electron spin excitations in a single "terbium double decker" molecule by rf-STS. (a) Zeeman diagram of the lowest $J_z = \pm 6$ substates of the $J = 6$ electronic ground state of the Tb^{3+} ion in $[TbPc_2]^-$; the hyperfine levels are labeled as $|J_z, I_z\rangle$; yellow, green, and blue arrows mark purely nuclear hyperfine transitions, labeled 1–3; grey arrows mark purely electronic transitions labeled 4 and 4'; red arrows mark mixed electronic nuclear transitions, labeled 5 and 5′. (b) Comparison of the calculated hyperfine transition frequencies of $TbPc_2$ (abscissa) with the experimental frequency values (ordinate) obtained by rf-STS on single $TbPc_2$ molecules on Au(111) at a static magnetic field of 2.5 mT (left) and 16 mT (right) perpendicular to the sample surface; boxes (open square) mark purely nuclear transitions; triangles (open triangle) mark transitions with electronic spin flips; the dashed line represents ideal agreement as guide to the eye; selected transitions marked by arrows in (a) are labeled 1–5, 4', and 5'; error bars are ±10% (horizontal) due to uncertainty of numerical parameters [20,22], ±0.05 GHz (vertical, open square) due to variable adsorption sites of different $TbPc_2$ molecules studied, and ±0.125 GHz (vertical, open triangle) due to the experimental uncertainty of the magnetic field of ±0.5 mT.

several orders of magnitude larger than, both, the cutoff frequency of the STM feedback loop and the bandwidth of the high-gain current amplifier of the STM. The maximum rf power level at the sample was −20 dBm, representing an adequate compromise between (i) achieving sufficiently large signals and (ii) avoiding Ohmic overheating of the sample, which compromises the stability of the TbPc2 molecule under the STM tip. On samples mounted to a conventional sample holder there was a magnetic field of 2.5 ± 0.5 mT at the sample due to the stray field of the magnetic tip holder of the STM instrument; a second sample holder was equipped with a permanent magnet producing a total magnetic field of 16 ± 0.5 mT at the sample. The respective field values are marked by dotted lines in Fig. 2(a).

For resonant spin excitation, the STM tip was placed at a fixed position over the phthalocyanine ligand of single $TbPc_2$ molecules at a constant tunneling current between 0.5 and 2 nA depending on tip stability. The sample voltage was set at +0.9 V, enabling electron tunneling from the STM tip into an unoccupied molecular orbital of the ligand of $TbPc_2$/Au(111) [11] as derived from Fig. 1(c), thereby charging the ligand negatively. The dc tunneling conductance, dI/dV, was measured while simultaneously modulating the sample bias at a variable radio frequency of 0.1–4.2 GHz. Figures 3(a) and 3(b) evidence that with the STM tip over the ligand of single $TbPc_2$ molecules, see position 1 of Fig. 1(b), we observe distinct peaks (increased dI/dV) at certain rf values growing clearly out of the base line. The data represent single-sweep spectra obtained within 30–60 s. Repeating the experiment with different STM tips and different $TbPc_2$ molecules adsorbed over different sites of the Au(111) lattice reproduces the dI/dV peaks within an experimental uncertainty of ±50 MHz. The intensities of the peaks are found to depend considerably on the STM tip, obscuring their dependence on the amplitude of the rf excitation. In addition, the frequency dependence of the transmission of the rf circuit complicates the analysis of absolute peak intensities in different frequency regimes. A comparison of the rf-STS spectra of Figs. 3(a) and 3(b), obtained at 2.5 and 16 mT, shows that some peaks strongly depend on the magnetic field (labeled 5, 5′), while others do not (labeled 1–3). In contrast, measuring over the bare Au substrate [position 2 in Fig. 1(b)] results in a constant dI/dV signal shown in Fig. 3(c). This confirms the dI/dV peaks of Figs. 3(a) and 3(b) originate from $TbPc_2$.

Peaks 1–3 appear in both spectra of Figs. 3(a) and 3(b) at almost the same frequencies of 2.2, 3.3, and 3.9 GHz, i.e., depending only very weakly on the magnetic field. They can be correlated with purely nuclear spin transitions of Tb^{3+} which exhibit a very weak Zeeman shift. Based on Ishikawa's model, the purely nuclear transitions 1–3—determined by the dipolar and quadrupolar hyperfine coupling constants—are calculated at frequencies of 2.4, 3.1, and 3.9 GHz. This is in reasonable agreement with the

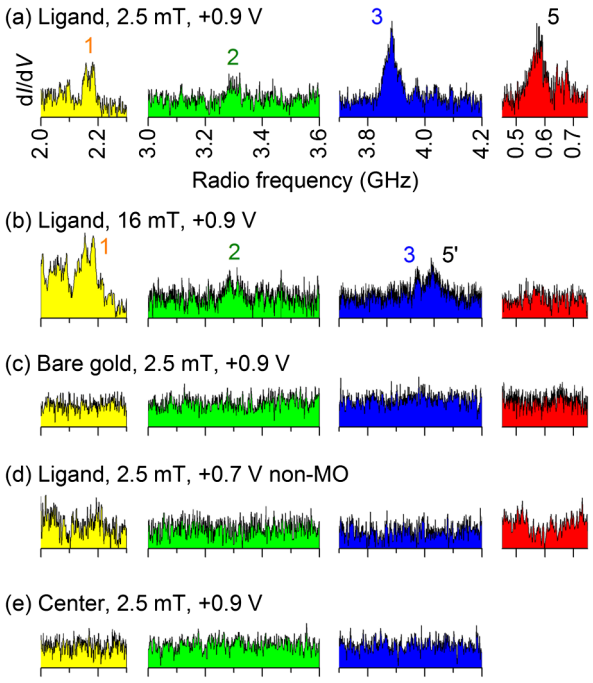

FIG. 3 (color online). Single-molecule spin resonance spectra by rf-STS. Conductance (dI/dV) spectra obtained by rf-STS over single $TbPc_2$ molecules adsorbed on Au(111) at 5 K, constant dc current between 0.5 and 2 nA, and 10 MHz/s rf sweep rate in different frequency ranges; the data represent single-sweep spectra acquired within 30–60 s; labels 1–3 and 5′ relate to selected spin transitions marked by arrows in Fig. 2(a); to compensate for the observed tip-dependence of the signal intensity, the spectra are normalized to a constant peak-to-peak fluctuation amplitude of the baseline noise. (a) STM tip placed over ligand [position 1 in Fig. 1(b)], static magnetic field of $B = 2.5$ mT applied perpendicular to the sample surface, dc sample bias voltage of $V_T = +0.9$ V for tunneling into unoccupied electronic state of $TbPc_2$ ligand. (b) Same as (a) with $B = 16$ mT. (c) Same as (a) but with tip placed over bare gold substrate [position 2 in Fig. 1(b)]. (d) Same as (a) but with $V_T = +0.7$ V for suppressing tunneling into $TbPc_2$ molecular orbitals. (e) Same as (a) with tip placed over the center of the adsorbed $TbPc_2$ molecule [position 3 in Fig. 1(b)].

experimental peak positions, as shown Fig. 2(b). Our results show that the hyperfine values used in Ishikawa's model for $[TbPc_2]^-$ anions in bulk phase are also appropriate for describing the spin structure of single $TbPc_2$ molecules adsorbed on Au(111) during rf-STS investigation. Small deviations may result from a weak interaction with the Au substrate, as indicated by the observed Kondo effect.

The purely electronic and mixed transitions, on the other hand, show a stronger dependence on the magnetic field. Unfortunately, we cannot tune the magnetic field to directly follow the B-field dependence of individual peaks. We therefore have plotted the experimental peaks obtained at two different values of the magnetic field in Fig. 2(b) against the calculated frequency values. Within the error bars of experiment and calculation [see caption of Fig. 2(b)], all data points lie on the dashed line (guide to the eye), thus revealing a stunningly good agreement for all observed frequencies with the calculated ones. The above results strongly evidence that the frequency values of the resonant dI/dV peaks observed by rf-STS, indeed, relate to the transition frequencies of different hyperfine levels of the Tb^{3+} ion in $TbPc_2$ adsorbed on Au(111). In comparison, no signatures of the magnetic moment of the Tb^{3+} ion have been detected by conventional dc-STM tunneling spectroscopy [11]. We remark, that the rich hyperfine structure of $TbPc_2$ helps to unambiguously interpret the experimental results, due to the large number of peaks that are all successfully identified by our rf-STS method. Furthermore, the resonance principle behind our rf-STS probe facilitates the detection of magnetic excitation energies as small as only a few μeV, i.e., 3 orders of magnitude below the mean thermal energy (few meV) of the sample at 5 K.

The presented rf-STS measurements reveal a novel (transport) mechanism, that couples the rf tunneling current to the electron and nuclear spin of the Tb^{3+} ion, and leads to an increase of the dc conductance in resonance. Recent studies have shown that the π-type electronic structure of phthalocyanine permits electronic coupling between the Tb^{3+} ion and the environment [11,35], providing a spin-dependent transport channel. Its conductance depends on the spin state of the Tb^{3+} ion, as shown for single $TbPc_2$ molecules in a molecular spin transistor [23] as well as in a supramolecular spin-valve geometry [22]. Our rf-STS experiments appear to utilize a similar transport mechanism. The important role of tunneling through the $TbPc_2$ ligand is supported by the absence of resonant peaks in the spectra of Figs. 3(d) and 3(e), where tunneling into the unoccupied molecular orbital is suppressed. In Fig. 3(d) the sample bias is off-resonant to the molecular orbital (+0.7 V) of $TbPc_2$, while in Fig. 3(e) the tip is placed over the center of the molecule [position 3 in Fig. 1(b)], where the respective spatial part of the MO wave function vanishes [36]. In both cases, no rf-induced dI/dV peaks are observed. A comparison of the spectra in Figs. 3(a) and 3(e), recorded at a lateral separation of ≈ 0.7 nm, evidences the subnanometer spatial resolution of our rf-STS method. The rf tunneling process is not restricted by the selection rules of photon-induced electromagnetic dipole transitions. The momentum conservation for spin excitation can be explained on the basis of three possible mechanisms for energy exchange processes between the Tb^{3+} ion and phonon radiation, including direct, Raman, and Orbach processes as discussed by Ishikawa *et al.* [21].

In conclusion, we successfully combined scanning tunneling spectroscopy with magnetic resonance principles into a new analysis technique, rf-STS, easily adaptable to a variety of nanoscale systems in the fields of nanoscience and nanotechnology. Our method enables the controlled resonant excitation and detection of electronic and nuclear spin transitions in single magnetic molecules. It

simultaneously offers single-spin sensitivity, submolecular spatial resolution, fast data acquisition, and electron-induced spin excitation unrestricted by the electromagnetic dipole selection rules. A sufficiently large coupling of the molecule's spin to its dc tunnel conductance (via opening of additional tunnel paths) is essential for observing rf-STS based spin resonance also in other types of magnetic molecules in the future. Rf-STS promises unprecedented possibilities for characterizing and controlling electron and nuclear spin excitations at the scale of single atoms and molecules, including resonance spectroscopy, addressing of spin-based quantum bits, and intramolecular analysis of chemical shifts.

We kindly acknowledge financial support of the project I958 by the Austrian Science Fund (FWF).

*Corresponding author.
stefan.muellegger@jku.at
†On sabbatical leave from the Department of Physics and Meteorology, Indian Institute of Technology, Kharagpur-721302, India.

[1] A. Abragam and B. Bleaney, *Electron Paramagnetic Resonance of Transition Ions* (Oxford University Press, Oxford, 1970).
[2] M. Levitt, *Spin Dynamics: Basics of Nuclear Magnetic Resonance* (Wiley, New York, 2001).
[3] L. Bogani and W. Wernsdorfer, Nat. Mater. **7**, 179 (2008).
[4] D. Gatteschi, R. Sessoli, and J. Villain, *Molecular Nanomagnets* (Oxford University Press, Oxford, 2006).
[5] D. Rugar, R. Budakian, H. J. Mamin, and B. W. Chui, Nature (London) **430**, 329 (2004).
[6] C. L. Degen, M. Poggio, H. J. Mamin, C. T. Rettner, and D. Rugar, Proc. Natl. Acad. Sci. U.S.A. **106**, 1313 (2009).
[7] M. S. Grinolds, M. Warner, K. De Greve, Y. Dovzhenko, L. Thiel, R. L. Walsworth, S. Hong, P. Maletinsky, and A. Yacoby, Nat. Nanotechnol. **9**, 279 (2014).
[8] T. Balashov, A. F. Takacs, W. Wulfhekel, and J. Kirschner, Phys. Rev. Lett. **97**, 187201 (2006).
[9] A. J. Heinrich, J. A. Gupta, C. P. Lutz, and D. M. Eigler, Science **306**, 466 (2004).
[10] S. Loth, M. Etzkorn, C. P. Lutz, D. M. Eigler, and A. J. Heinrich, Science **329**, 1628 (2010).
[11] T. Komeda, H. Isshiki, J. Liu, Y. F. Zhang, N. Lorente, K. Kato, B. K. Breedlove, and M. Yamashita, Nat. Commun. **2**, 217 (2011).
[12] D. Fang, H. Kurebayashi, J. Wunderlich, K. Vyborny, L. P. Zarbo, R. P. Campion, A. Casiraghi, B. L. Gallagher, T. Jungwirth, and A. J. Ferguson, Nat. Nanotechnol. **6**, 413 (2011).
[13] Y. Manassen, R. J. Hamers, J. E. Demuth, and A. J. Castellano, Jr., Phys. Rev. Lett. **62**, 2531 (1989).
[14] T. Komeda and Y. Manassen, Appl. Phys. Lett. **92**, 212506 (2008).
[15] Y. Sainoo, H. Isshiki, S. M. F. Shahed, T. Takaoka, and T. Komeda, Appl. Phys. Lett. **95**, 082504 (2009).
[16] Y. Manassen, I. Mukhopadhyay, and N. R. Rao, Phys. Rev. B **61**, 16223 (2000).
[17] C. Durkan and M. E. Welland, Appl. Phys. Lett. **80**, 458 (2002).
[18] N. Ishikawa, M. Sugita, T. Ishikawa, S. Koshihara, and Y. Kaizu, J. Am. Chem. Soc. **125**, 8694 (2003).
[19] N. Ishikawa, M. Sugita, T. Okubo, N. Tanaka, T. Iino, and Y. Kaizu, Inorg. Chem. **42**, 2440 (2003).
[20] N. Ishikawa, M. Sugita, and W. Wernsdorfer, Angew. Chem., Int. Ed. Engl. **44**, 2931 (2005).
[21] N. Ishikawa, M. Sugita, T. Ishikawa, S. Koshihara, and Y. Kaizu, J. Phys. Chem. B **108**, 11265 (2004).
[22] M. Urdampilleta, S. Klyatskaya, M. Ruben, and W. Wernsdorfer, Phys. Rev. B **87**, 195412 (2013).
[23] R. Vincent, S. Klyatskaya, M. Ruben, W. Wernsdorfer, and F. Balestro, Nature (London) **488**, 357 (2012).
[24] S. Thiele, R. Vincent, M. Holzmann, S. Klyatskaya, M. Ruben, F. Balestro, and W. Wernsdorfer, Phys. Rev. Lett. **111**, 037203 (2013).
[25] S. Thiele, F. Balestro, R. Ballou, S. Klyatskaya, M. Ruben, and W. Wernsdorfer, Science **344**, 1135 (2014).
[26] S. Stoll and A. Schweiger, J. Magn. Reson. **178**, 42 (2006).
[27] A. De Cian, M. Moussavi, J. Fischer, and R. Weiss, Inorg. Chem. **24**, 3162 (1985).
[28] M. Gonidec, D. B. Amabilino, and J. Veciana, Dalton Trans. **41**, 13 632 (2012).
[29] S. Müllegger, M. Rashidi, K. Mayr, M. Fattinger, A. Ney, and R. Koch, Phys. Rev. Lett. **112**, 117201 (2014).
[30] S. Müllegger, A. K. Das, K. Mayr, and R. Koch, Nanotechnology **25**, 135705 (2014).
[31] W. Chen, V. Madhavan, T. Jamneala, and M. F. Crommie, Phys. Rev. Lett. **80**, 1469 (1998).
[32] K. Katoh, Y. Yoshida, M. Yamashita, H. Miyasaka, B. K. Breedlove, T. Kajiwara, S. Takaishi, N. Ishikawa, H. Isshiki, Y. F. Zhang, T. Komeda, M. Yamagishi, and J. Takeya, J. Am. Chem. Soc. **131**, 9967 (2009).
[33] Y.-S. Fu, J. Schwöbel, S.-W. Hla, A. Dilullo, G. Hoffmann, S. Klyatskaya, M. Ruben, and R. Wiesendanger, Nano Lett. **12**, 3931 (2012).
[34] K. J. Franke, G. Schulze, and J. I. Pascual, Science **332**, 940 (2011).
[35] A. Lodi Rizzini, C. Krull, T. Balashov, J. J. Kavich, A. Mugarza, P. S. Miedema, P. K. Thakur, V. Sessi, S. Klyatskaya, M. Ruben, S. Stepanow, and P. Gambardella, Phys. Rev. Lett. **107**, 177205 (2011).
[36] Y. Kitagawa, T. Kawakami, A. Yamanaka, and M. Okumura, Mol. Phys. **112**995 (2014).